Wood Science and Technology
https://doi.org/10.1007/s00226-023-01498-y

ORIGINAL

Ionic liquid, ultrasound-assisted synthesis of lignin nanoparticles for barrier-enhanced all-cellulose nanocomposite films

Elahe Amini[1] · Cristina Valls[1] · M. Blanca Roncero[1]

Received: 24 April 2023 / Accepted: 11 September 2023

Abstract

The primary purpose of this work was to develop novel all-cellulose nanocomposite (ACNC) films by following a green approach that uses an ionic liquid as solvent and requires no additional reducing agents or stabilizers. In this way, biodegradable, UV-blocking ACNC films were obtained by partially dissolving cellulose to entrap lignin nanoparticles (LNP) within. Lignin particles in proportions of 3–7 wt% were modified by sonication in an ionic liquid (IL) to obtain lignin-IL dispersions. The influence of the LNP-IL medium on the chemical, physical, and morphological properties of the resulting nanocomposites was examined, and the properties compared with those of an all-cellulose composite (ACC) film and untreated paper. The TEM technique revealed the formation of unevenly spherical LNPs as small as 5.133 ± 0.003 nm, and XRD spectroscopy a transition from cellulose I to II and an increase in the proportion of non-crystalline cellulose as a result of partial dissolution and regeneration. In addition, SEM images confirmed the deposition of LNPs onto the surface of the regenerated cellulose matrix. The incorporation of LNPs considerably enhanced the UV-blocking, oxygen and water-barrier, biodegradation, antioxidant and antibacterial properties of the films. Moreover, LNPs in proportions of 3 and 5 wt% increased tensile strength, and a proportion of 7 wt% allowed the films to block 97% of light at 280 nm and increased antioxidant activity by 68% relative to the control sample. Interestingly, a 7 wt% LNP content in the films decreased antibacterial activity against *Staphylococcus aureus* and *Escherichia coli* by about 42.85% and 63.88%, respectively. The new, multifunctional biocomposite films are suitable for various uses in cellulose-based food packaging.

✉ Elahe Amini
elahe.amini@upc.edu

[1] CELBIOTECH_Paper Engineering Research Group, Universitat Politècnica de Catalunya (UPC), Colom 11, 08222 Terrassa, Barcelona, Spain

Published online: 05 October 2023

Introduction

Cellulose which accounts for over 1.5 trillion tons of biomass output each year (Zhang et al. 2016), is one of the most abundant renewable biopolymers on the planet. Its biodegradability, renewability, biocompatibility and non-allergenicity make it a highly suitable material for a variety of purposes (Luo et al. 2019). Cellulose-based multifunctional composites, which have spurred a rise in the use of green materials, provides a way of addressing specific environmental pollution due to plastics.

All-cellulose composites (ACC) constitute a novel class of monocomposites using cellulosic material as both matrix and reinforcing phase, which consist of non-crystalline and undissolved cellulose, respectively (Ghaderi et al. 2014; Amini et al. 2021).

All-cellulose composites, which were introduced by Takashi et al. (2004), can be obtained via two different routes, namely (1) a two-step process by which a portion of cellulose is completely dissolved for subsequent mixing with an additional, reinforcing cellulosic material (He et al. 2014; Zhang et al. 2016); and (2) a single-step process involving partial dissolution of the cellulosic material followed by in situ regeneration to obtain a matrix phase wrapping the undissolved fibre core (Takashi et al. 2004; Yousefi et al. 2011).

In recent years, highly transparent all-cellulose composites have been deemed the ideal biocomposites for use in structural and packaging materials, filters, and photoelectric and biomedical engineering devices, on the grounds of their outstanding properties, which include biodegradability, high mechanical strength and optical transparency (Amini et al. 2021). Cellulose is insoluble in most common solvents and resistant to degradation by virtue of the rigid hydrogen-bonding networks formed within and between molecular chains, and its partially crystalline structure (Ryu et al. 2017). Therefore, increasing its accessibility entails opening up its inner pores and cavities (lumens and pits) in addition to disrupting fibril aggregates and highly ordered regions (Amini et al. 2023b). A number of common solvents including dimethylacetamide/LiCl (Takashi et al. 2004; Yousefi et al. 2015), NMMO (Ouajai and Shanks 2009), ionic liquids (Yousefi et al. 2011) and NaOH-urea (Piltonen et al. 2016) have been used to dissolve cellulose fibres. Moreover, a number of researchers have sought to develop a sustainable, environmentally friendly process for dissolving cellulose.

Ionic liquids (ILs), which are liquid salts with a melting point below 100 °C, are efficient green solvents for cellulose. In fact, ILs possess unique physicochemical properties including high solvent power, good thermal stability, recyclability, high thermal and chemical stability, low toxicity, non-flammability and miscibility with many other solvents, all of which make them effective alternatives to potentially hazardous chemicals (Amini et al. 2023a).

Industries are increasingly seeking novel bio-based UV-blocking materials containing UV absorbers that enable exposure to UV light over long periods. Lignin has attracted much attention as a UV absorbent for boosting the UV-blocking performance of cellulosic materials without sacrificing recyclability,

biodegradability or biocompatibility (Wei et al. 2020). Furthermore, lignin is the second most abundant natural material after cellulose, with an annual production of 50 million tons as waste during the pulping process, for example. This makes it a highly available, low-cost biomass resource. However, only 2% of lignin waste is currently recovered for use in chemical and material applications (Borrega et al. 2020). As a result, lignin has become a highly desirable target for researchers and industries.

Specifically, micro- and nanolignin materials have opened up promising new avenues for obtaining high added value, environmentally friendly bio-based materials (Deng et al. 2021). Lignin nanoparticles (LNPs) contain functional (phenol, ketone) groups and chromophores with excellent UV-blocking properties, and possess antibacterial and antioxidant activity (Rukmanikrishnan et al. 2020b), which may make them effective substitutes for metal oxides in the production of UV-blocking biocomposite films on the grounds of their increased surface-to-volume ratio and predictably enhanced interaction with the polymer matrix (Garcia Gonzalez et al. 2017).

Sonication is a commonplace treatment for liquids containing particles. It is a green technique that can be used to break large particles into smaller ones in order to facilitate deagglomeration and ensure high dispersion in a matrix (Ghauri et al. 2020). Garcia Gonzalez et al. (2017) examined the effect of sonication on softwood kraft lignin with a view to obtaining lignin nanoparticles (LNPs) of excellent colloidal stability for use in bio-based nanocomposite materials. In this way, they obtained LNPs ranging from approximately 10–50 nm in size.

Ionic liquids have been used as effective media to ensure adequate dispersion and the synthesis of various types of nanoparticles thanks to their monodispersive and non-agglomerative properties (Verma et al. 2019; Montalbán et al. 2018). ILs provide electrostatic insulation in the form of a "protective shell" for nanoparticles that helps stabilize them through their cations and/or anions without the need for additional stabilizers, surfactants or covering ligands (Aditya et al. 2018).

In this work, we developed a simple method for preparing transparent all-cellulose nanocomposite films reinforced with lignin nanoparticles in an ionic liquid medium. The method uses 1-ethyl-3-methylimidazolium acetate (EmimAc) as solvent to obtain a disordered phase on the surface of cellulose, the cellulose being subsequently regenerated to ensure nanowelding of fibres and entrapment of nanoparticles (Fig. 1). Combining the ionic liquid with sonication enables uniform distribution of the resulting lignin nanoparticles and dispenses with the need for reducing agents or stabilizers. The influence of the amount of nanoparticles present on the mechanical strength, and the antioxidant, antimicrobial activity, UV-blocking, and water vapor and oxygen barrier properties of the resulting nanocomposite films, was examined. As shown by the results, the proposed method provides a straightforward, environmentally friendly approach to producing bio-based nanocomposite films reinforced with lignin nanoparticles as fully bioderived fillers that are suitable for advanced nanocomposite applications.

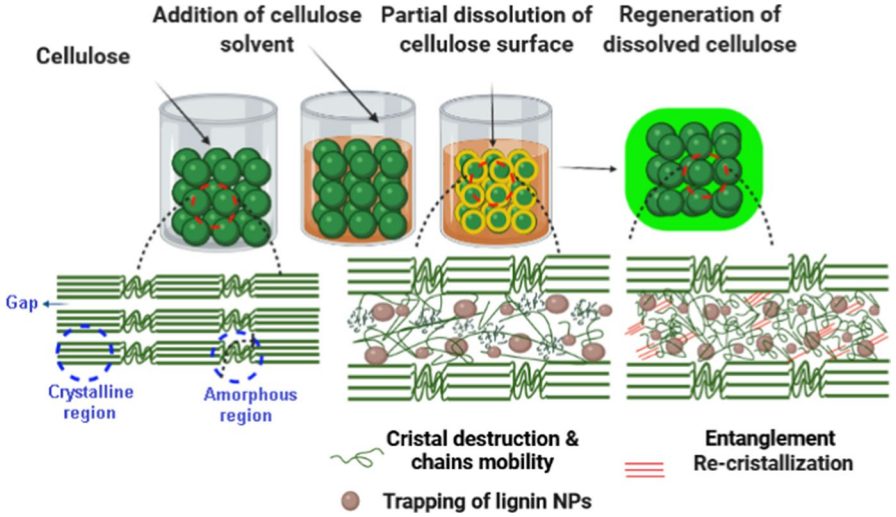

Fig. 1 Treatment of bleached paper with IL and impact on micro- and nanostructures

Materials and methods

Materials

The cellulose source used was highly purified bleached fibre of cotton linter pulp supplied by Celsur (Granada, Spain). The pulp contained more than 90% α-cellulose as calculated according to TAPPI T203. The ionic liquid, 1-ethyl-3-methylimidazolium acetate (EmimAc), was supplied in 98% purity by Sigma-Aldrich (Darmstadt, Germany) and removed with distilled water when needed. Sulphonated kraft lignin powder of molecular weight (M_w)= 46500 g/mol and a total sulphur content of 6.9% was obtained from Borregaard (Sarpsborg, Norway).

Preparation of an all-cellulose nanocomposite film

The original paper was obtained from cotton linter pulp containing more than 90% α-cellulose according to ISO 5269-2 on a Rapid-Köthen machine. Moist paper was then sandwiched between two stacks of standard filter paper and compressed at 0.1 MPa at 90 °C for 10 min. Based on preliminary research and previous reports (Zou et al. 2022; Garcia Gonzalez et al. 2017), variable amounts of lignin (3, 5 and 7 wt% of paper) were dispersed in 3 mL of ionic liquid and sonicated at room temperature (25 °C), a frequency of 20 kHz and a power of 130 W for 30 min to obtain homogeneous, stable nanodispersions. The starting cellulosic material and the glassware used were carefully dried to avoid any adverse effects of water on cellulose dissolution.

The required amount of dried paper (aerial weight 40 g/m^2, area 64 cm^2) was placed in a glass Petri dish after preparing the nanolignin-IL solution to be used as nanowelding and UV-blocking agent for application to the paper surface. In order to boost IL-assisted partial dissolution of cellulose, the process was allowed to continue in an oven at 80 °C for 24 h. After dissolution, the resulting gel nanocomposite films were removed from the oven and allowed to cool at room temperature. Then, each film was washed by coagulation in de-ionized water to obtain a transparent nanocomposite gel, residual ionic liquid present in the regenerated sample being removed by washing several times. Next, each film was sandwiched between two glass plates and oven-dried at 60 °C for 1 h. Finally, the nanocomposite was blotted between filter paper and glass plate to dry at 50% relative humidity (RH) at 25 °C for at least 3 days. The all-cellulose composite film used as control sample was obtained by following the above-described procedure in the absence of lignin nanoparticles. The nanocomposite films obtained from 3, 5 and 7 wt% LNPs were coded ACNC3%LNPs, ACNC5%LNPs and ACNC7%LNPs, respectively.

Characterization

Transmission electron microscopy (TEM)

The transmission electron microscopy was used to determine the size and morphology of the particles. A Philips TECNAI 10 electron microscope was used and operated at 100 kV with a digital camera Megaview II. The sample was subjected to a treatment with osmium tetroxide to provide it with a higher electronic density. Subsequently, it was dehydrated with ethanol and included in EPON resin. To obtain the ultrathin sections, a SORVALL MT2-B ultramicrotome with a Diatome 45º diamond blade was used. Ultrathin sections were deposited on a formvar-supported 200 mesh copper grid.

Fourier transform infrared spectroscopy (FTIR)

Fourier transform infrared spectra were performed using an FTIR spectrophotometer (Spectrum 100, Perkin Elmer, USA). Spectra were acquired within 4000–600 cm^{-1} region, using 64 scans overlapped and 1 cm^{-1} resolution. The results of the spectra were normalized.

X-ray diffraction (XRD)

The X-ray diffraction patterns of the nanocomposite films were recorded using an X-ray diffractometer (PANalytical X'Pert PRO MPD Alpha1 powder diffractometer in a Bragg-Brentano $\theta/2\theta$ geometry of 240 mms of radius). The samples were analyzed at the radiation wavelength of 1.5406 Å and 45 kV-40 mA with the scanning range of 2°–60° (2θ). The crystallinity index (CI) was calculated according to the following Eq. (1) (Segal et al. 1959):

$$\mathrm{CrI}\ (\%) = \frac{(I_2 00 - I_a m)}{I_2 00} \times 100 \tag{1}$$

where $I_2 00$ is the intensity of the peak assigned to the (200) reflection of cellulose Iβ, which is typically in the range 2θ= 21–23°. $I_a m$ is the minimum in the intensity occuring at about 2θ=18° for noncrystalline cellulose. The Scherrer's Eq. (2) was used for estimating the crystallite size:

$$D = \frac{K/\lambda}{\beta/\cos\theta} \tag{2}$$

where K is the constant of 0.9, λ is the wavelength of the incident X-ray (0.154056 nm), β is the FWHM (Full width at half maximum) of the diffraction peak in radians, and θ is the diffraction angle corresponding to the planes (Lu et al. 2017).

Scanning electron microscopy (SEM)

The surface and cross section of obtained nanocomposite films were observed by means of FE-SEM (model JSM-7100F, JEOL, USA) using an accelerating voltage of 10 kV. Prior to characterization, the samples were coated with a thin conducting layer of graphite to avoid electrical charging during the observation.

Antioxidant activity

The antioxidant activity of ACNC films was determined using the stable radical 2,2′-azinobis-(3-ethylbenzothiazoline-6-sulfonic acid) ($ABTS^+$), according to the modified method of Amini et al. (2023a, 2023b). A spectroscopic approach based on the disappearance of the free radical $ABTS^+$'s absorption band at 752 nm was used to test the free radical scavenging activity in this method. Briefly, the $ABTS^+$ solution was made by oxidation of potassium persulfate. The solution was diluted to obtain an absorbance of 0.70 ± 0.1 at 752 nm. For comparison, 10 mg of sample was added to 1.5 mL of $ABTS^+$ solution and vortexed about 2 min. Afterward, the sample was centrifuged 4 min at 6000 rpm. Finally, the sample was maintained at room temperature in the dark for 30 min and the absorbance was measured at 752 nm. The absorbance of control sample was also measured at 752 nm in the same procedure. This analysis was performed at least 5 times for each sample. The antioxidant activity of the nanocomposite film was calculated according to the following Eq. (3):

$$\text{Antioxidant activity}\ (\%) = \frac{(A_o - A_1)}{A_o} \times 100 \tag{3}$$

where A_o is the absorbance of control (without sample) and A_1 is the absorbance of nanocomposite film sample.

Antimicrobial activity

Bacterial reduction on the functionalized samples was investigated against *E. coli* as the model Gram-negative bacteria and *S. aureus* as the model Gram-positive bacteria, according to the standard method, ASTM E 2149–01 "standard test method for determining the antimicrobial activity of immobilized antimicrobial agents under dynamic contact conditions." The reduction of bacterial growth was determined as $R(\%)$ reduction using the following Eq. (4):

$$R\,(\%) = \frac{(A - B)}{A} \times 100 \tag{4}$$

where A and B are the number of bacteria colony-forming units (CFU/ml) after contact with the test samples and without samples grown on agar plates under the same conditions.

Optical properties

L^* (lightness), a^* (redness-greenness) and b^* (yellowness-blueness) as the color parameters were determined using a colorimeter (Technidyne, UK). A white plate was used as a standard for color measurement ($L = 92.92$) and color parameters were calculated at three random positions on the surface of the film. The total color difference ($\triangle E$) between each color value of the standard color plate and film sample was obtained according to this following Eq. (5):

$$\triangle E = \sqrt{(L^* - L)^2 + (a^* - a)^2 + (b^* - b)^2} \tag{5}$$

Ultraviolet and visible light barrier properties of the films were determined at wavelengths between (200–800 nm) using a UV–visible spectrophotometer (Evolution 600, Thermo Scientific) as described by Mohammadi et al. (2018). Firstly the samples were cut into rectangular strips (1 cm × 3 cm) and then directly placed into the quartz cuvette; the measurement of each film sample was taken three times with air as the control.

Water contact angle (WCA)

Optical contact angle meter (OCA15EC, Dataphysics Co., USA) was used to measure the hydrophobicity of film surface, using an image capture ratio of 25 frame/s. Square films with a size of 1 cm × 5 cm and a 5 µL droplet of distilled water were placed on the film surface using a microsyringe (Hamilton, Switzerland) and a needle (0.75 mm diameter). The WCA was performed within 0–60 s and the digital images were taken after 1 s. At least five replicates were performed for each formulation.

Water vapor permeability (WVP) and oxygen transmission rate (OTR)

The WVP of the nanocomposite film was measured gravimetrically according to the weight gain method stated in the ASTM E96/E96M-16 standard with slight modification. For the measurement, the samples were first conditioned using a humidity chamber controlled at 25 °C and 50%RH with an air movement of 198 m/min. Then, the sample was installed on a standard cup filled with 3 g of calcium chloride ($CaCl_2$) salt and sealed by hot glue stick and parafilm to avoid water vapor penetration. The entire set, after weighing, was placed at 25 ± 2 °C and 98 ± 2 %RH, and the cup was weighed every 24 h periodically for 48 h. In order to calculate water vapor transmission rate (WVTR) in ($g \cdot m^{-2} \cdot day^{-1}$), the slope was obtained from a chart of weight gain vs. time using a simple linear regression method. By dividing the slope of each line by the surface of the sample exposed to water vapor, WVTR was determined, according to the following Eq. (6):

$$\mathrm{WVTR} = \frac{(G/t)}{A} = \frac{\mathrm{slope}}{\mathrm{test\ area}} \tag{6}$$

Finally, the WVP of the sample was measured using the following Eq. (7) (Amini et al. 2023a):

$$\mathrm{WVP} = \frac{\mathrm{WVTR}}{P(R_1 - R_2)} \times X \tag{7}$$

where X is the film thickness (m), P is the saturation vapour pressure of water at 25 °C (Pa), $R1$ is the relative humidity in the chamber (98% RH), and $R2$ is the relative humidity in the cups (0% RH).

The oxygen transmission rate (OTR) of the film was measured by an (MOCON OX-TRAN Model 1/50, USA) oxygen permeability tester. The film sample with an area of 50 cm^2 was tested at two different test conditions, 23 °C, 0% RH and 38 °C, 90% RH, in 24 h.

Thickness measurement and mechanical properties

The film thickness measurement was performed by a micrometer (Frank-PTI digital 16502, Germany), according to ISO 534:2011. At least five random locations of each film sample were measured. The mechanical properties of different formulations were determined with a universal testing machine (JJ Lloyd instrument, model T5K) equipped with a 500 N load cell, and a crosshead speed of 50 mm/min. Film samples were cut into rectangular shape with 40 mm length and 15 mm width. Prior to mechanical testing, the films were conditioned for at least one week at 25 °C and under 50 %RH. Mechanical parameters, i.e., tensile strength (TS), elongation at break (EB) and Young's modulus (YM), were obtained from five replicates for each film formulation directly from the resulting stress–strain curves.

Biodegradation test

The biodegradation tests of samples and cellophane were performed in soil at ambient temperature under moisture-controlled conditions (Zhao et al. 2019). The samples were cut into 200 × 200 mm and dried completely before tests. The initial weight of the samples was also recorded. Then, the compost soil was put in a plastic box. Thereafter, the samples were buried about 2 cm beneath soil which was regularly moistened with distilled water. After that, the samples were taken out at predetermined time points for 6 weeks and rinsed with distilled water in order to ensure the stop of the degradation. At least five replicates were performed for each formulation. The final weight was measured and the weight loss of the sample degraded in soil at 7-day intervals was calculated according to the following Eq. (8):

$$\text{Weight loss } (\%) = \frac{(W_o - W_1)}{W_o} \times 100 \tag{8}$$

where W_0 is the initial weight of the original specimen and W_1 is the final weight of dry sample exposed to the soil for a certain time.

Results and discussion

TEM

The lignin nanoparticles obtained with sonication in the ionic liquid were examined by high-resolution transmission electron microscopy. Figure 2 shows the TEM images for an all-cellulose nanocomposite (ACNC) film containing 7 wt% nanoparticles of average size 5.133 ± 0.003 nm. The images confirm that sonication enabled the formation of nanosized lignin particles that were unevenly spherical in shape. Therefore, as previously found by Aditya et al. (2018), the ionic liquid provided an excellent medium for their preparation. Thus, it enhanced electronic and steric stabilization of the nanoparticles, and reduced particle growth by effect of its constituent anion and cation forming a protective electrostatic shell that prevented agglomeration (Verma et al. 2019; Montalbán et al. 2018).

FTIR spectroscopy

FTIR spectroscopy was used to examine structural changes in cellulose from the raw material to the ACC and ACNC films. As can be seen from Fig. 3, all exhibited the typical broad bands over the wavenumber range 3000–3650 cm^{-1} due to stretching vibrations of OH groups in cellulose. O–H vibrations in the base paper appeared at 3336 cm^{-1}, whereas those in the nanocomposite films containing some or no LNPs were observed at 3440 and 3490 cm^{-1}, respectively.

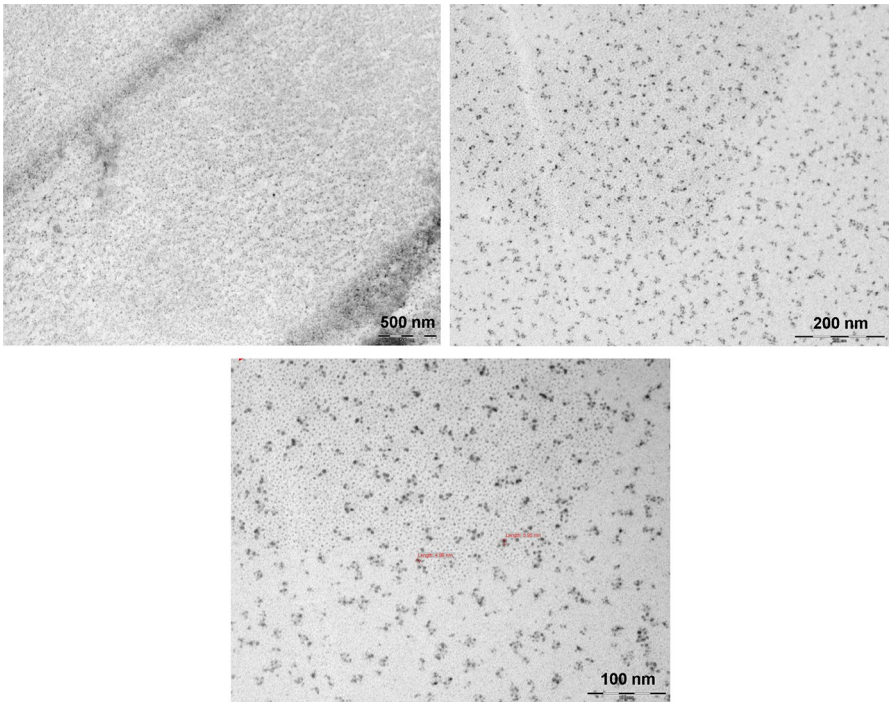

Fig. 2 TEM images at different magnifications of an all-cellulose nanocomposite film containing 7% lignin nanoparticles

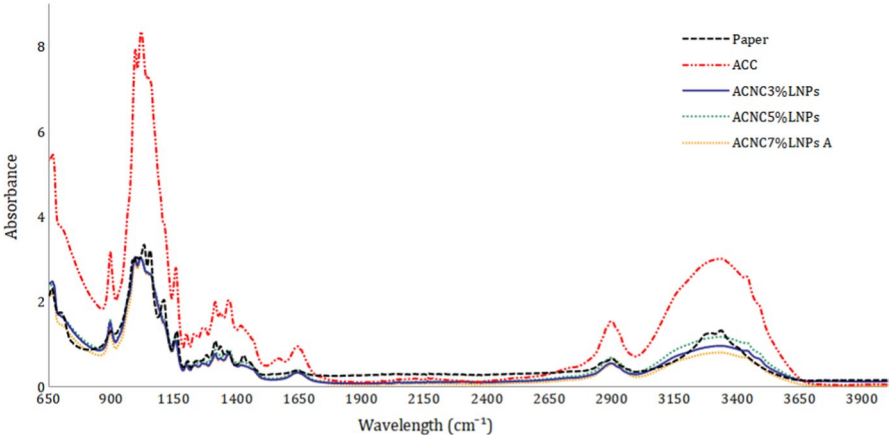

Fig. 3 FTIR spectra for paper, the ACC film and all-cellulose nanocomposite films containing different amounts of lignin nanoparticles

According to Xu et al. (2010), the shift in the O–H vibration bands results mainly from the cleavage of hydrogen bonds. The peak for OH vibrations in regenerated cellulose containing no LNPs was higher than those for the films containing nanoparticles.

Lignin nanoparticles probably blocked interactions between cellulose and EmimAc to some extent, thereby increasing the ability of the ionic liquid to break intermolecular and intramolecular hydrogen bonds relative to the IL/LNPs solvent system (Yang et al. 2019). Conversion of cellulose I into cellulose II caused the bands at 1430 and 1110 cm^{-1} for the former in ACC and ACNC reinforced with dissolved cellulose to be flattened, which suggests a prevalence of crystalline cellulose (cellulose II; Zhu et al. (2018)). Also, the spectra exhibited similar characteristic bands, so the macromolecular structure of cellulose was not destroyed by dissolution or regeneration (Amini et al. 2023a, 2023b; Yang et al. 2019). Overall, no new absorption peaks were observed in the FTIR spectra for the ACNC films, which suggests that no new chemical bonds were formed even after adding LNPs in a proportion of 3–5%. This in turn suggests that the nanoparticles were compatible with the cellulose matrix. Similar results were previously reported for chitosan films containing LNPs (Zou et al. 2022).

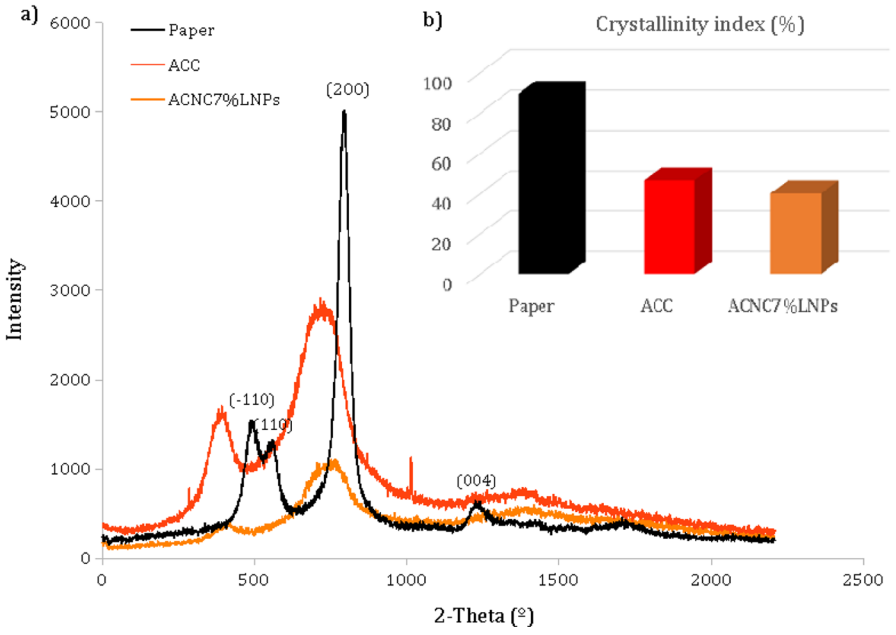

Fig. 4 XRD patterns for the paper, ACC film and all-cellulose nanocomposite film with a 7% content in lignin nanoparticles

X-ray diffraction spectroscopy

Figure 4a shows the XRD patterns for the original paper, ACC film and ACNC film with the highest content in lignin nanoparticles, and Fig. 4b their changes in crystallinity index and crystallite size. As can be seen, the XRD spectrum for the base paper exhibited lines for cellulose I at the 2θ values 22.8°, 34.6°, 14.8° and 16.6° on the 200, 004, – 110 and 110 crystal plane, respectively. After dissolution and regeneration, the spectrum exhibited additional lines for regenerated cellulose at 12.2° (– 110) and 20.7° (110), which correspond to cellulose II (Yang et al. 2019).

As can be seen, the crystal structure of cellulose was altered by partial dissolution and regeneration. The ACC films with and without LNPs had the same crystal structure as cellulose II. This result suggests that LNPs did not alter the crystal structure of the regenerated cellulose matrix. The crystallinity index (CrI) and crystallite size of base paper were considerably lower in the ACC film (46.58% and 1.50 nm, respectively, versus 89.36% and 6.75 nm, respectively). Therefore, the crystal structure of cellulose I changed to amorphous cellulose upon dissolution in the ionic liquid. These results suggest that the solvent penetrated gaps and partially dissolved cellulose crystallites Amini et al. (2023a, 2023b). The crystallinity index and crystallite size of the film containing 7% LNPs were considerably lower than those of the control film, a result that can be ascribed to weaker interaction of LNPs with cellulose chains leading to a less cohesive structure.

Surface morphology

The surface of the ACNC films was examined in SEM images. The original paper had a very open, porous structure consisting of randomly intertwined fibers (Fig. 5a and b). On the other hand, the ACC film, which was partially dissolved, exhibited a uniform, compact, relatively smooth surface without aggregates (Fig. 5c and d).

Interfacial compatibility between the reinforcing phase (undissolved cellulose fibres) and the reinforced matrix in the ACC film was excellent because both consisted of cellulose. The matrix provides partial mechanical strength and acts as a binder to weld the reinforcing phase together. The surface of the ACC film contained micro- and nanoholes suitable for embedding LNPs. The distribution of LNPs in the regenerated cellulose matrix of the ACNC film with the highest LNP content was examined. Increasing the amount of LNPs in the ACC film was found to cause filling of most microholes and cavities in the cellulose matrix (Fig. 5e). At the nanoscale level, the welding agent successfully caused nanofibres to bind to one another by penetrating deeply into the nanogaps between nanofibrils (Fig. 5f and g). This result is consistent with previous reports of Yousefi et al. (2011) and Amini et al. (2023b) on the nanowelding/joining effect of partial dissolution of nano/microcellulose in an ionic liquid.

Antioxidant activity

Antioxidants, which are free-radical scavengers that neutralize reactive oxygen species (ROS) produced during aerobic cell metabolism, have gained growing interest

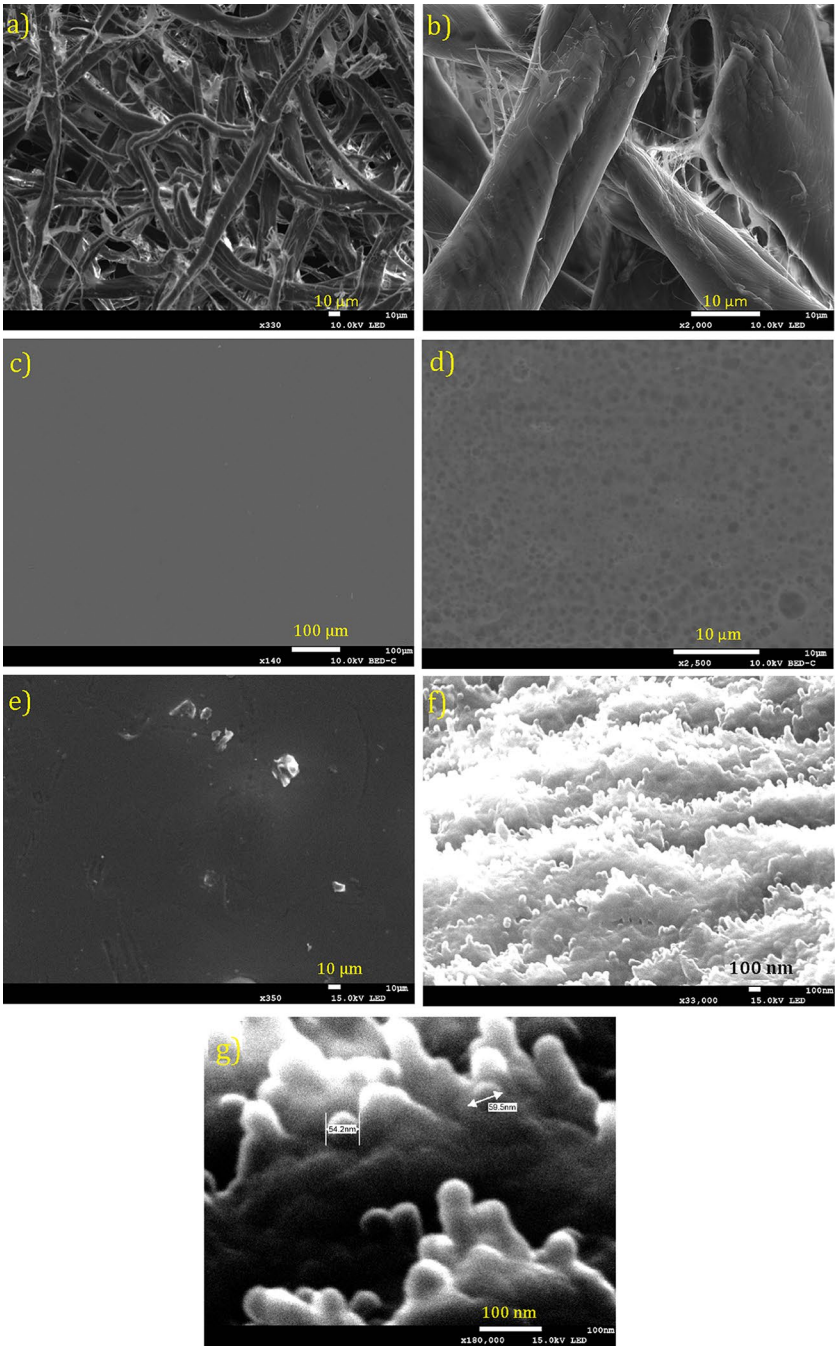

Fig. 5 SEM images at different magnifications illustrating the surface morphology of the paper (**a**, **b**), ACC film (**c**, **d**) and ACNC7%LNPs (**e**–**g**)

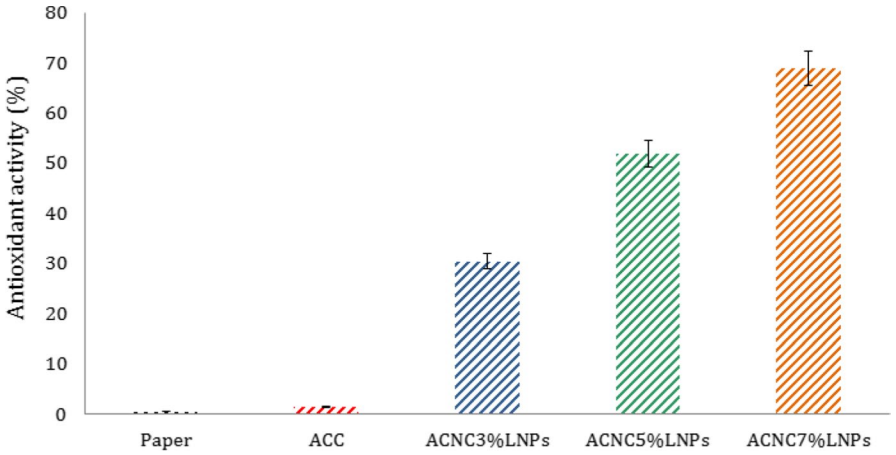

Fig. 6 Antioxidant activity of paper, the ACC film and all-cellulose nanocomposite films with different contents in lignin nanoparticles

as film components. Free radicals can be harmful to both biotic and abiotic entities (Găman et al. 2020). Antioxidant activity in the ACNC films was assessed with the ABTS radical scavenging method. As can be seen from Fig. 6, the antioxidant activity of the nanocomposite films was substantially improved by incorporation of lignin nanoparticles. In contrast, the paper and the ACC film exhibited little antioxidant activity by effect of exposed electron-releasing hydroxyl groups in the cellulose matrix reacting with free radicals over time (Priyadarshi et al. 2021).

A prior study showed a cellulose-based film to possess limited antioxidant activity (Priyadarshi et al. 2021). However, other reports suggest that lignin possesses antioxidant activity by effect of its containing phenolic hydroxyl groups that effectively reduce or inhibit free radicals by virtue of their hydrogen-releasing ability which makes lignin a useful antioxidant for nanocomposite films (Tian et al. 2017). In fact, increasing the proportion of LNPs in the nanocomposite films boosted antioxidant activity. Thus, the film containing 3 wt% LNPs had a considerably increased activity (30.46%) and that containing 7% LNPs an even higher one (68.97%). Therefore, LNPs seemingly provide a safe, inexpensive way of enhancing the antioxidant activity of films with a view to producing materials with improved properties.

Antimicrobial activity

S. aureus and *E. coli* are among the most common bacterial contaminants encountered in foodstuff. By targeting these bacteria, antibacterial packaging can be freed of major sources of foodborne contamination and the shelf life of the food it contains extended (Gutiérrez et al. 2012).

Table 1 shows the antibacterial activity against *S. aureus* and *E. coli* of the ACC film, as control sample, and that of ACNC films containing variable amounts of LNPs. As can be seen, antibacterial activity in the ACNC films increased with increasing content in LNPs. In fact, LNPs introduced further active functional groups

Table 1 Count of colony-forming units against *S. aureus* and *E. coli* in the ACC film and in all-cellulose nanocomposite films with different contents in lignin nanoparticles

	Reduction (%)			
	ACC (0%LNPs)	3%LNPs	5%LNPs	7%LNPs
S.aureus	1.45	15.71	27.85	42.85
E.coli	5.55	17.80	30.55	63.88

(e.g., aliphatic OH, carbonyl CO, COOH, sulphur) in the film structure, which likely contributed to enhancing the antibacterial properties of the film (Alzagameem et al. 2019). The results also indicate that the nanocomposite films were effective against both bacteria. The control sample exhibited little antibacterial activity, with microbe counts less than 5% in both species. Adding 3% LNPs to the films increased reduction of *S. aureus* and *E. coli* to 15.71% and 17.80%, respectively. However, such small reductions suggest that the film ACNC3%LNPs was inefficient against both bacteria. Antibacterial activity was considerably higher in ACNC7%LNPs, which exhibited a reduction of 42.85% in *S. aureus* and of 63.88% in *E. coli*.

Previous studies showed microbial growth to be inhibited by phenolic groups in lignin. Also, the presence of lignin nanoparticles further increased antimicrobial activity by effect of their high surface area providing better contact with microbes (Wang et al. 2019; Yang et al. 2021). Growth of Gram-negative bacteria such as *E. coli* is usually easier to stop than is that of Gram-positive bacteria such as *S. aureus*, probably as a result of the difference in the cell wall structure between the two. Thus, Gram-negative bacteria have more complex cell walls consisting of lipids, proteins and lipopolysaccharides (LPS), which can make them more susceptible to some antimicrobial agents. On the other hand, Gram-positive bacteria possess an additional protective layer in the form of a dense peptidoglycan cell wall that provides effective defense against some biocides and makes them generally more resistant to antimicrobial treatments (Amini et al. 2016; Babaee et al. 2022). For instance, Yang et al. (2018) found LNPs from alkaline lignin to be effective against Gram-negative bacteria, possibly as a result of (1) polyphenols damaging (lysing) bacterial cell walls; and (2) small nanoparticles penetrating bacterial cells and depleting adenosine triphosphate (ATP) by infiltration (Yang et al. 2018; Huang et al. 2020).

Optical properties

As can be seen from Fig. 7, EmimAc is one of the best ILs for homogeneous dissolution of cellulosic materials and production of highly transparent films. The substantial transparency of the ACC and ACNC films may have resulted from mobilization of cellulose fibres, and plasticization at surface level reducing light scattering and widening the band gap of the films (Reyes et al. 2018).

ACNC films additionally exhibited a visually uniform distribution of lignin. Consumers tend to favor transparent food packaging. ACNC films are transparent but gradually develop a light brown colour that alters their optical properties (see Table 2). The color parameters compared here included.

Fig. 7 Appearance and qualitative transparency of ACNC nanocomposite films with different contents in lignin nanoparticles

L^* (lightness), a^* (green–red), b^* (blue–yellow) and $\triangle E$ (total color difference). The ACC film had an L^*, a^* and b^* value of 88.75, −1.32 and 3.25, respectively. L^* decreased slightly with increasing lignin content, whereas b^* was greater than the value for the ACC film. The nanocomposite films containing 5% and 7% LNPs exhibited similar L^* values (86.11 and 86.78, respectively). The $\triangle E$ values for the ACNC films containing 3, 5, and 7% LNPs were 4.24%, 6.20%, 7.82% and 9.78%, respectively. Therefore, ACNC7%LNPs was the film with the highest $\triangle E$ value as a result of the typical brown colour of lignin (Haqiqi et al. 2021; Hararak et al. 2021).

A number of organic compounds are degraded by UV. As a result, UV-blocking films are appealing as packaging materials, and the conjugated structure of lignin imparts a substantial UV-blocking ability to cellulose films (Ma et al. 2022). Transmittance of UV and visible light through the ACNC films was assessed here at 280 and 660 nm, respectively.

As can be seen from Table 2, the ACC film exhibited poor UV blocking performance. In contrast, the films containing LNPs showed excellent UV-blocking properties, their performance increasing with increase in LNP content. In fact, UV-blocking by ACNC3%LNPs, ACNC5%LNPs and ACNC7%LNPs was 57.33%, 70.43% and 93.31%, respectively. Similarly to a neat ACC film, ACNC3%NLPs exhibited low UV protection with high transmittance in the visible region. Moreover, visible light transmittance was sacrificed with higher proportions of LNPs owing to the colour of lignin itself (Hararak et al. 2021). The light blocking ability of the films can thus seemingly be ascribed to the presence of substantial amounts of

Table 2 Colour, light transmittance (%) and transparency of the cellulose nanocomposite films

Sample	Color				Light transmittance (%) at different wavelength (nm)		Thickness (μm)
	L (lightness)	*a* (green–red)	*b* (blue–yellow)	△*E* (total color difference)	280	660	
ACC	88.75 ± 0.05	− 1.32 ± 0.03	3.25 ± 0.05	4.24 ± 0.15	81.90 ± 0.76	85.42 ± 0.42	48 ± 2.05
ACNC3%NLPs	87.48 ± 0.13	− 1.59 ± 0.01	5.45 ± 0.06	6.20 ± 0.11	42.67 ± 3.25	83.91 ± 1.85	57.00 ± 5.65
ACNC5%NLPs	86.78 ± 0.12	− 1.81 ± 0.05	7.29 ± 0.05	7.82 ± 0.25	29.57 ± 1.28	80.60 ± 3.25	62.66 ± 7.76
ACNC7%NLPs	86.111 ± 0.34	− 1.96 ± 0.06	10.18 ± 0.61	9.78 ± 0.62	6.69 ± 1.74	75.84 ± 3.40	63.00 ± 2.82

unsaturated structures (phenol and ketone groups in addition to other chromophores) in lignin nanoparticles. These results are consistent with those of previous studies that demonstrated the UV-shielding ability of LNPs, particularly when incorporated into cellulose-based films (Posoknistakul et al. 2020; Cao et al. 2021). In general, the nanoparticles provided an effective barrier against UV light while maintaining excellent transparency in the films, which is essential for packaging foods and light-sensitive products.

Water contact angle

Knowing the surface properties of cellulosic materials can help develop packaging materials for specific purposes from them. The water contact angle (WCA) is a measure of the affinity of lignin for an ACC surface. We thus made WCA measurements of the ACNC films to assess their hydrophilicity or hydrophobicity. The results are shown in Fig. 8. A film with WCA > 90° is deemed hydrophobic (Haqiqi et al. 2021). All films studied here had WCA < 90°, so they were classified as hydrophilic. The highest WCA (69°) was that for ACNC7%LNPs and the lowest one (36.4°) that for ACC (i.e., the film containing no lignin). WCA increased gradually with increase in LNP content of the ACNC films, which can be ascribed to the hydrophobic nature of lignin.

The hydrophobicity of lignin is imparted mainly by its ester groups by contrast, the hydrophilicity of pure cellulose is a result of its abundant hydroxyl groups. Lignin nanoparticles can be made more hydrophobic through formation of reverse micelles and exposure of their aromatic surface skeletons, thereby further increasing WCA (Qian et al. 2015; Bai et al. 2022). Therefore, consistent with the results of previous studies by Wang et al. (2021) and Teh et al. (2021), incorporating LNPs

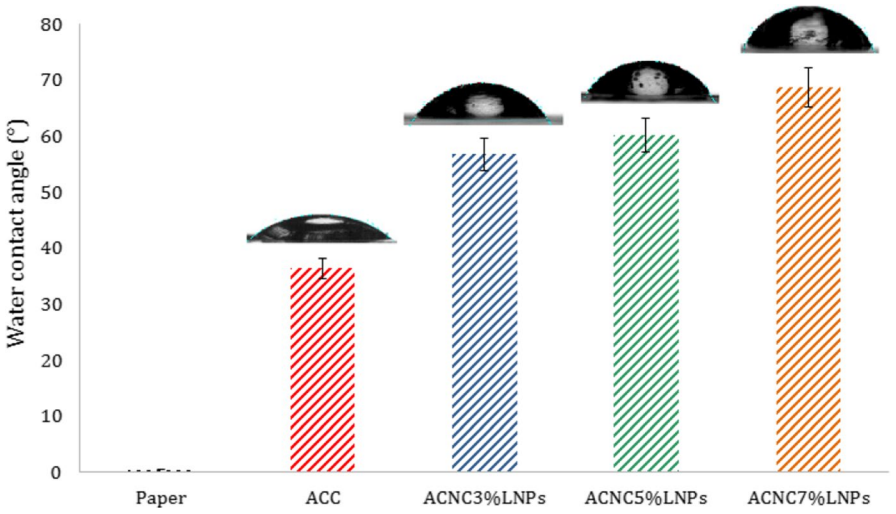

Fig. 8 Water contact angle of the paper, ACC film and all-cellulose nanocomposite films with different contents in lignin nanoparticles

into an ACC film can be expected to hinder access of water to regenerated cellulose fibres and broaden the scope of ACC films in food contact packaging.

Water vapor permeability and oxygen transmission rate

The influence of the LNP content of the films on their water vapour and oxygen barrier properties was investigated. The water vapor permeability (WVP) of the ACC film was 8.67×10^{-9} g· m^{-1} · h^{-1}.Pa^{-1} and lower than that of the paper. This result suggests that the ionic liquid enhanced the water barrier properties of the films (see Fig. 9). The remarkable barrier properties of ACC can be ascribed to the multilayered, highly packed nanostructures it contains. During its formation, polymer chains entangle with other, similarly disintegrated chains by forming cohesive bonds throughout the rinsing and drying stages (Yousefi et al. 2011, 2015). Adding 7% LNPs to the regenerated cellulose matrix substantially decreased WVP (from 8.67 to 6.25×10^{-9} g· m^{-1} · h^{-1}.Pa^{-1}, which was better than the value for the ACNC film containing 3% LNPs (Michelin et al. 2020). Shankar et al. (2015) previously found adding LNPs to agar composite films to reduce their WVP, possibly because of strong intermolecular interactions between agar and lignin molecules leading to a more tortuous path for diffusion of water vapour and fewer water molecules permeating through the polymer film as a result.

Figure 10 shows the oxygen permeability (OTR) at 0% and 90% RH of the ACNC films. Clearly, partial dissolution in the ionic liquid considerably decreased OTR. Moreover, incorporating lignin into the film formulation resulted in a significant

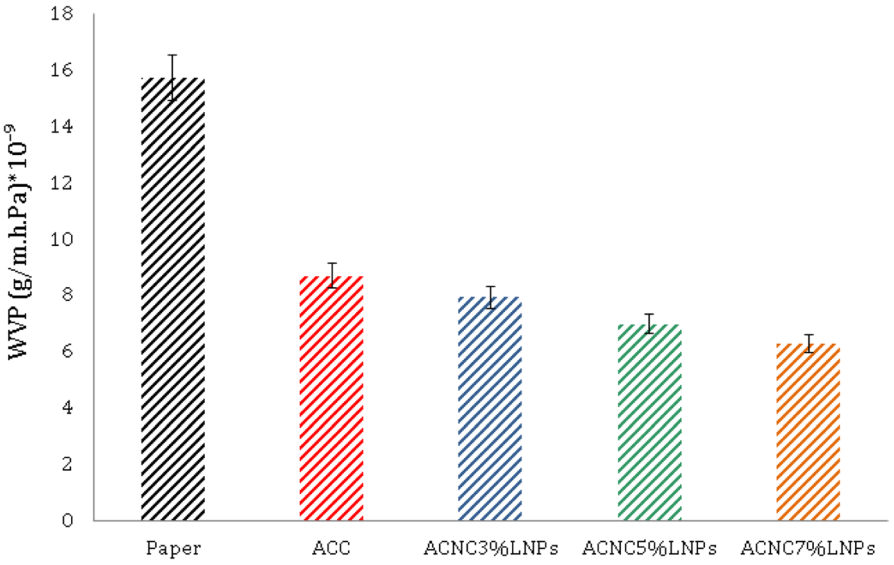

Fig. 9 Water vapour permeability (WVP) of the paper, ACC film and all-cellulose nanocomposite films with different contents in lignin nanoparticles

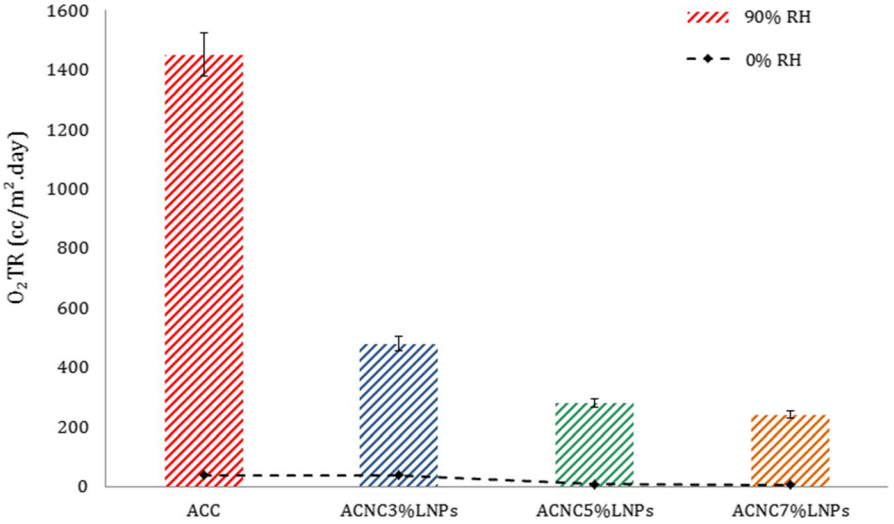

Fig. 10 OTR for the ACC film and all-cellulose nanocomposite films with different contents in lignin nanoparticles

difference. Thus, at 0% RH, both ACC and ACNC3%LNPs exhibited an identical OTR value (38.25); also, ACNC5%LNPs and ACNC7%LNPs provided a completely impenetrable barrier for oxygen, thus confirming that using lignin as a small molecular filler successfully increases the density of composite films (Ma et al. 2022). At 90% RH, the films exhibited poorer barrier properties. This was a result of cellulose fibrils easily absorbing water and swelling at a high relative humidity, thereby causing further breakage of fibril-fibril bonds in the films by effect of the high polarity of the fibrils (Luo et al. 2021). At 90% RH, increasing the LNP content to 7 wt% decreased OTR by 84.38% relative to the ACC film. Similar results were previously reported by Zou et al. (2022), who found adding nanolignin to polymer matrices to reduce oxygen and water vapour permeability by effect of the films being more compact and containing fewer voids.

Film thickness and mechanical properties

As can be seen from Table 2, the welding effect of the ionic liquid reduced film thickness relative to the original paper (from 122 ± 4.08 to 48 ± 2.05μm in the ACC film). This was a result of the welding agent (IL) providing a more compact surface for macrofibres in the original paper. The thickness of the ACC films increased with increasing content in LNPs.

Figure 11 summarizes the mechanical properties of ACNC films with variable amounts of lignin nanoparticles in terms of Young's modulus (YM), tensile strength (TS) and elongation at break (EB). TS, which was 0.6 MPa for untreated paper, increased 134-fold after dissolution in the ionic liquid. The increase can be ascribed to the ionic liquid acting as a nanowelding agent and causing the formation of a tighter network with more junction points by connecting smaller fibres in

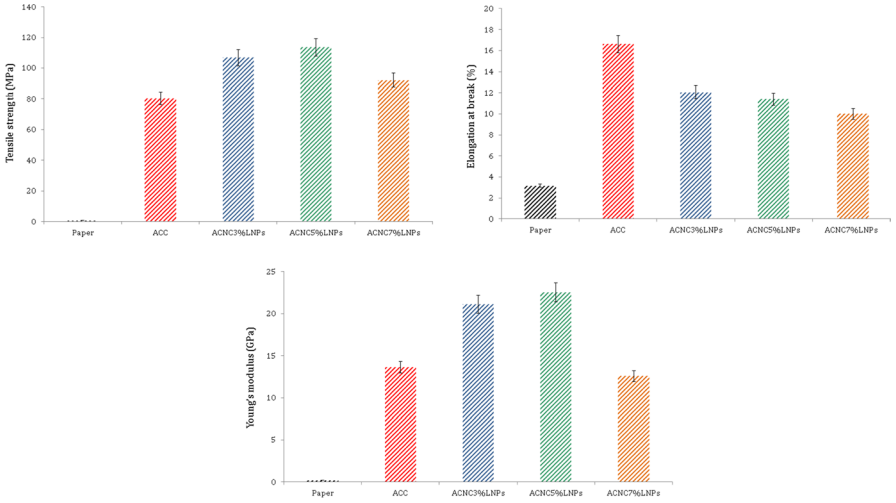

Fig. 11 Tensile strength (MPa), elongation at break (%) and Young's modulus (GPa) of the paper, ACC film and all-cellulose nanocomposite films with different contents in lignin nanoparticles

the nanostructures. Cellulose fibre surfaces were most likely plasticized by effect of the ionic liquid also acting as a plasticizer and increasing ductility as a result. This outcome is consistent with previous conclusions of Ghaderi et al. (2014) and Amini et al. (2023a,b). Here, TS for the ACC film was altered by addition of LNPs. In fact, TS and YM for the ACNC films containing up to 5%LNPs were substantially greater (113.59 MPa and 22.51 GPa, respectively). An et al. (2021) previously found TS for cellulose-based films to increase upon incorporation of lignin. However, further addition of LNPs to our films (to a 7 wt% content) dramatically decreased TS and YM (to 92.19 MPa and 12.56 GPa, respectively). The decrease in both parameters may have resulted from non-uniform dispersion and agglomeration of LNPs in the regenerated cellulose matrix (Shankar et al. 2015). These results are consistent with those of the WVP test. In addition, elongation at break was smaller in the LNP-containing ACNC films than in the ACC film. The decreased elongation break resulting from the addition of LNPs can be ascribed to the aromaticity of lignin and its increased structural stiffness relative to the cellulose matrix hindering motion of macromolecular chains in cellulose (Shankar et al. 2015; Rukmanikrishnan et al. 2020a). An et al. (2021) also found lignin to reduce EB in cellulose-based films.

Biodegradability

Biodegradability in the ACC and ACNC films was assessed by burying them in soil for 6 weeks. Weight loss is a major proxy for the ease with which biocomposite films can be degraded in the environment. Figure 12 shows the weight loss of the films as measured at regular intervals. Degradation was very slow in all samples after the first week. Thus, the loss of the ACNC film in the second week was 4–6% greater than those of the ACC film (3.57%) and the paper (only 2.5%). ACNC7%LNPs

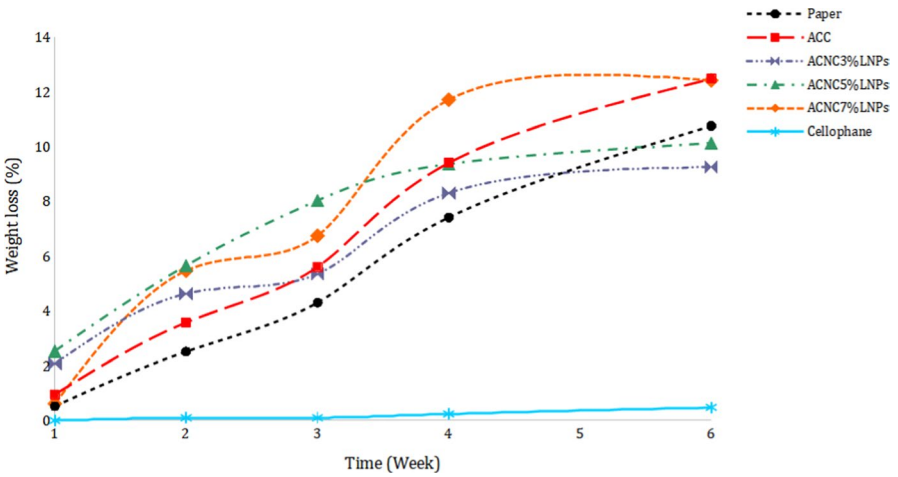

Fig. 12 Biodegradation results of paper, ACC and all cellulose nanocomposite films at different contents of lignin nanoparticles

exhibited the greatest weight loss (almost 12 wt%) after 4 weeks. The ACC film also experienced a marked loss after the fourth week, possibly as a consequence of its porous structure allowing water to penetrate into the polymer network and weaken bonds as a result. After 6 weeks, the weight loss of the ACC film and the paper was about 12.5% and 11%, respectively. These values exceeded those for the ACNC3%LNPs and ACNC5%LNPs (9.25% and 10%, respectively). By contrast, the loss of ACNC7%LNPs was essentially similar to that of the ACC film.

Lignin has been ascribed antimicrobial properties by virtue of its containing aromatic alcohol structures (Dudeja et al. 2023). Such properties were enhanced by a high lignin content in the films, which is consistent with the weaker tendency of ACNC films to degrade after 5 weeks of burial in soil. Also, the ACC film exhibited a higher biodegradation rate relative to the paper sample as the likely result of its degradability being strongly influenced by the crystallinity of cellulose. Crystalline zones are more difficult to degrade. The crystallinity indices found were consistent with biodegradation of the samples. Thus, the cellophane weight loss after 5 weeks was only 0.47%, so degradation of this material was negligible probably because of the additives it typically contains hindering the process (Zhao et al. 2019).

Conclusion

All-cellulose nanocomposite films containing different amounts of lignin nanoparticles (LNPs) were prepared by using a simple ultrasound, IL-assisted method and then examined for morphological, surface, optical, antimicrobial, mechanical and antioxidant properties. Based on the results, lignin nanoparticles imparted UV-shielding, biodegradation, antioxidant and antibacterial properties to the ACC film, particularly at the higher filler loadings studied. Thus, the 5%LNPs formulation

exhibited excellent tensile strength, Young's modulus, and barrier properties (OTR and WVP). The nanoparticles also altered surface hydrophobicity in the films. Adding LNPs to the regenerated cellulose matrix had no substantial effect on light transmission, however. Partial dissolution and regeneration did alter the crystal structure of cellulose judging by the XRD patterns for the films. Moreover, the ACC film was structurally identical to cellulose II films containing some or no LNPs.

TEM images of the lignin nanoparticles showed them to be unevenly spherical and disperse, but not aggregated, at the nanoscale. In addition, their FTIR spectra and SEM images revealed good compatibility with the surface of the regenerated cellulose matrix. SEM images also revealed that addition of LNPs and their gap-filling effect made the cellulose-based film more compact and homogeneous. The LNP content needed to maximize the physico-mechanical properties of the cellulose matrix was 5%. Based on the results, ACNC films obtained in the presence of an ionic liquid and LNPs are expected to facilitate the development of novel, effective multifunctional bio-based materials.

Acknowledgements This research received financial support from the PID2020-114070RB-I00 (CELLECOPROD) project [MCIN/AEI/10.13039/501100011033]. The first author, E. Amini, gratefully acknowledges the Universitat Politècnica de Catalunya and Banco Santander for the financial support of her predoctoral grant FPI-UPC.

Author contributions All authors contributed to the study conception and design. Material preparation, data collection and analysis were performed by EA. The first draft of the manuscript was written by EA and all authors commented on previous versions of the manuscript. All authors read and approved the final manuscript.

Funding Open Access funding provided thanks to the CRUE-CSIC agreement with Springer Nature.

Data availability All data generated or analyzed during this study are included in this published article.

Declarations

Conflict of interest The authors declare that they have no known competing financial interests or personal relationships that could have influenced the work reported in this paper.

Ethical approval Not applicable.

References

Aditya A, Chattopadhyay S, Jha D et al (2018) Zinc oxide nanoparticles dispersed in ionic liquids show high antimicrobial efficacy to skin-specific bacteria. ACS Appl Mater Interfaces 10(18):15401–15411

Alzagameem A, Klein SE, Bergs M et al (2019) Antimicrobial activity of lignin and lignin-derived cellulose and chitosan composites against selected pathogenic and spoilage microorganisms. Polymers 11(4):670

Amini E, Azadfallah M, Layeghi M et al (2016) Silver-nanoparticle-impregnated cellulose nanofiber coating for packaging paper. Cellulose 23:557–570

Amini E, Valls C, Roncero MB (2021) Ionic liquid-assisted bioconversion of lignocellulosic biomass for the development of value-added products. J Clean Prod 326:129275

Amini E, Valls C, Roncero MB (2023a) Promising nanocomposites for food packaging based on cellulose-PCL films reinforced by using ZNO nanoparticles in an ionic liquid. Ind Crops Prod 193:116246

Amini E, Valls C, Yousefi H et al (2023) Ionic liquid/ZNO assisted preparation of high barrier cellulose nanocomposite films by in situ ring-opening polymerization of lactide monomers. J Polym Environ 31(6):2576–2594

An L, Chen J, Heo JW et al (2021) Synthesis of lignin-modified cellulose nanocrystals with antioxidant activity via diels-alder reaction and its application in carboxymethyl cellulose film. Carbohydr Polym 274:118651

Babaee M, Garavand F, Rehman A et al (2022) Biodegradability, physical, mechanical and antimicrobial attributes of starch nanocomposites containing chitosan nanoparticles. Int J Biol Macromol 195:49–58

Bai Y, Wang X, Wang X et al (2022) Self-assembled/composited lignin colloids utilizing for therapy, cosmetics and emulsification. Front Chem 10:1107643

Borrega M, Paarnila S, Greca LG et al (2020) Morphological and wettability properties of thin coating films produced from technical lignins. Langmuir 36(33):9675–9684

Cao X, Huang J, He Y et al (2021) Biodegradable and renewable UV-shielding polylactide composites containing hierarchical structured poss functionalized lignin. Int J Biol Macromol 188:323–332

Deng J, Sun SF, Zhu EQ et al (2021) Sub-micro and nano-lignin materials: small size and rapid progress. Ind Crops Prod 164:113412

Dudeja I, Mankoo RK, Singh A et al (2023) Development, characterisation and biodegradability of rice straw lignin based sustainable biopolymeric films. Int J Food Sci Technol 58(5):2754–2763

Găman AM, Egbuna C, Găman MA (2020) Natural bioactive lead compounds effective against haematological malignancies. Phytochem Lead Compd New Drug Discov 95–115

Garcia Gonzalez MN, Levi M, Turri S et al (2017) Lignin nanoparticles by ultrasonication and their incorporation in waterborne polymer nanocomposites. J Appl Polym Sci 134(38):45318

Ghaderi M, Mousavi M, Yousefi H et al (2014) All-cellulose nanocomposite film made from bagasse cellulose nanofibers for food packaging application. Carbohydr Polym 104:59–65

Ghauri A, Ghauri I, Elhissi AM et al (2020) Characterization of cochleate nanoparticles for delivery of the anti-asthma drug beclomethasone dipropionate. Advances in medical and surgical engineering. Elsevier, Amsterdam, pp 267–277

Gutiérrez D, Delgado S, Vázquez-Sánchez D et al (2012) Incidence of staphylococcus aureus and analysis of associated bacterial communities on food industry surfaces. Appl Environ Microbiol 78(24):8547–8554

Haqiqi MT, Bankeeree W, Lotrakul P et al (2021) Antioxidant and UV-blocking properties of a carboxymethyl cellulose-lignin composite film produced from oil palm empty fruit bunch. ACS Omega 6(14):9653–9666

Hararak B, Winotapun C, Inyai J et al (2021) Production of UV-shielded spherical lignin particles as multifunctional bio-additives for polyvinyl alcohol composite films. J Nanoparticle Res 23(8):1–15

He X, Xiao Q, Lu C et al (2014) Uniaxially aligned electrospun all-cellulose nanocomposite nanofibers reinforced with cellulose nanocrystals: scaffold for tissue engineering. Biomacromolecules 15(2):618–627

Huang C, Dong H, Zhang Z et al (2020) Procuring the nano-scale lignin in prehydrolyzate as ingredient to prepare cellulose nanofibril composite film with multiple functions. Cellulose 27(16):9355–9370

Lu P, Cheng F, Ou Y et al (2017) Rapid fabrication of transparent film directly from wood fibers with microwave-assisted ionic liquids technology. Carbohydr Polym 174:330–336
Luo J, Zhang M, Yang B et al (2019) A promising transparent and UV-shielding composite film prepared by aramid nanofibers and nanofibrillated cellulose. Carbohydr Polym 203:110–118
Luo J, Su Y, Chen J et al (2021) Pretreatment of lignin-containing cellulose micro/nano-fibrils (lcmnf) from corncob residues. Cellulose 28(8):4671–4684
Ma L, Zhu Y, Huang Y et al (2022) Strong water-resistant, UV-blocking cellulose/glucomannan/lignin composite films inspired by natural lcc bonds. Carbohydr Polym 119083
Michelin M, Marques AM, Pastrana LM et al (2020) Carboxymethyl cellulose-based films: effect of organosolv lignin incorporation on physicochemical and antioxidant properties. J Food Eng 285:110107
Mohammadi R, Mohammadifar MA, Rouhi M et al (2018) Physico-mechanical and structural properties of eggshell membrane gelatin-chitosan blend edible films. Int J Biol Macromol 107:406–412
Montalbán MG, Carissimi G, Lozano-Pérez AA et al (2018) Biopolymeric nanoparticle synthesis in ionic liquids. Recent Adv Ion Liq 3–26
Ouajai S, Shanks RA (2009) Preparation, structure and mechanical properties of all-hemp cellulose biocomposites. Compos Sci Technol 69(13):2119–2126
Piltonen P, Hildebrandt NC, Westerlind B et al (2016) Green and efficient method for preparing all-cellulose composites with naoh/urea solvent. Compos Sci Technol 135:153–158
Posoknistakul P, Tangkrakul C, Chaosuanphae P et al (2020) Fabrication and characterization of lignin particles and their ultraviolet protection ability in pva composite film. ACS Omega 5(33):20976–20982
Priyadarshi R, Kim SM, Rhim JW (2021) Carboxymethyl cellulose-based multifunctional film combined with zinc oxide nanoparticles and grape seed extract for the preservation of high-fat meat products. Sustain Mater Technol 29:e00325
Qian Y, Qiu X, Zhong X et al (2015) Lignin reverse micelles for UV-absorbing and high mechanical performance thermoplastics. Ind Eng Chem Res 54(48):12025–12030
Reyes G, Borghei M, King AW et al (2018) Solvent welding and imprinting cellulose nanofiber films using ionic liquids. Biomacromolecules 20(1):502–514
Rukmanikrishnan B, Rajasekharan SK, Lee J et al (2020a) K-carrageenan/lignin composite films: biofilm inhibition, antioxidant activity, cytocompatibility, UV and water barrier properties. Mater Today Commun 24:101346
Rukmanikrishnan B, Ramalingam S, Rajasekharan SK et al (2020b) Binary and ternary sustainable composites of gellan gum, hydroxyethyl cellulose and lignin for food packaging applications: biocompatibility, antioxidant activity, uv and water barrier properties. Int J Biol Macromol 153:55–62
Ryu MH, Park J, Oh DX et al (2017) Precisely controlled two-step synthesis of cellulose-graft-poly (l-lactide) copolymers: effects of graft chain length on thermal behavior. Polym Degrad Stab 142:226–233
Segal L, Creely JJ, Martin A Jr et al (1959) An empirical method for estimating the degree of crystallinity of native cellulose using the x-ray diffractometer. Textile Res J 29(10):786–794
Shankar S, Reddy JP, Rhim JW (2015) Effect of lignin on water vapor barrier, mechanical, and structural properties of agar/lignin composite films. Int J Biol Macromol 81:267–273
Takashi N, Ikuyo M, Koichi H (2004) All-cellulose composite. Macromolecules 37(20):7683–7687
Teh KC, Foo ML, Ooi CW et al (2021) Sustainable and cost-effective approach for the synthesis of lignin-containing cellulose nanocrystals from oil palm empty fruit bunch. Chemosphere 267:129277
Tian D, Hu J, Bao J et al (2017) Lignin valorization: lignin nanoparticles as high-value bio-additive for multifunctional nanocomposites. Biotechnol Biofuels 10(1):1–11
Verma C, Ebenso EE, Quraishi M (2019) Transition metal nanoparticles in ionic liquids: synthesis and stabilization. J Mol Liq 276:826–849
Wang X, Wang S, Liu W et al (2019) Facile fabrication of cellulose composite films with excellent UV resistance and antibacterial activity. Carbohydr Polym 225:115213
Wang Y, Liu S, Wang Q et al (2021) Strong, ductile and biodegradable polylactic acid/lignin-containing cellulose nanofibril composites with improved thermal and barrier properties. Ind Crops Prod 171:113898
Wei Z, Cai C, Huang Y et al (2020) Strong biodegradable cellulose materials with improved crystallinity via hydrogen bonding tailoring strategy for UV blocking and antioxidant activity. Int J Biol Macromol 164:27–36

Xu A, Wang J, Wang H (2010) Effects of anionic structure and lithium salts addition on the dissolution of cellulose in 1-butyl-3-methylimidazolium-based ionic liquid solvent systems. Green Chem 12(2):268–275

Yang J, Lu X, Yao X et al (2019) Inhibiting degradation of cellulose dissolved in ionic liquids via amino acids. Green Chem 21(10):2777–2787

Yang W, Fortunati E, Gao D et al (2018) Valorization of acid isolated high yield lignin nanoparticles as innovative antioxidant/antimicrobial organic materials. ACS Sustain Chem Eng 6(3):3502–3514

Yang W, Ding H, Qi G et al (2021) Enhancing the radical scavenging activity and UV resistance of lignin nanoparticles via surface mannich amination toward a biobased antioxidant. Biomacromolecules 22(6):2693–2701

Yousefi H, Nishino T, Faezipour M et al (2011) Direct fabrication of all-cellulose nanocomposite from cellulose microfibers using ionic liquid-based nanowelding. Biomacromolecules 12(11):4080–4085

Yousefi H, Mashkour M, Yousefi R (2015) Direct solvent nanowelding of cellulose fibers to make all-cellulose nanocomposite. Cellulose 22(2):1189–1200

Zhang J, Luo N, Zhang X et al (2016) All-cellulose nanocomposites reinforced with in situ retained cellulose nanocrystals during selective dissolution of cellulose in an ionic liquid. ACS Sustain Chem Eng 4(8):4417–4423

Zhao G, Lyu X, Lee J et al (2019) Biodegradable and transparent cellulose film prepared eco-friendly from durian rind for packaging application. Food Packag Shelf Life 21:100345

Zhu R, Liu X, Song P et al (2018) An approach for reinforcement of paper with high strength and barrier properties via coating regenerated cellulose. Carbohydr Polym 200:100–105

Zou Z, Ismail BB, Zhang X et al (2022) Improving barrier and antibacterial properties of chitosan composite films by incorporating lignin nanoparticles and acylated soy protein isolate nanogel. Food Hydrocolloids 108091